BBAA VI International Colloquium on:
Bluff Bodies Aerodynamics & Applications
Milano, Italy, July, 20-24 2008

A NEW GENERAL 3DOF QUASI-STEADY AERODYNAMIC INSTABILITY MODEL.

Henrik Gjelstrup[*x], Allan Larsen[*], Christos Georgakis[x] and Holger Koss[x]

[*]COWI A/S, Parallelvej 2, 2800 Kgs. Lyngby , Denmark
e-mails: hegj@cowi.dk, aln@cowi.dk

[x]BYG•DTU, Building 118, Brovej, 2800 Kgs. Lyngby , Denmark
e-mails: heg@byg.dtu.dk, cg@byg.dtu.dk, hko@byg.dtu.dk

Keywords: Aerodynamic instability criterion, Aerodynamic damping, Bluff body

Abstract

This paper proposes a three degrees of freedom (3DOF) quasi-steady aerodynamic model and an instability criterion for a bluff body, which is uniform along the length axis. The model and criterion has been developed in the frame of investigating aerodynamic instability of cables due to ice accretions but can generally be applied for aerodynamic instability prediction for prismatic bluff bodies. The 3DOF, which make up the movement of the model, are the displacements in the XY-plane and the rotation around the bluff body's rotational axis. The proposed model incorporates inertia coupling between the three degrees of freedom and is capable of estimating the onset of aerodynamic instability for changes in drag, lift and moment, which is a function of wind angle of attack (α) in relation to the x-axis of the bluff body, Reynolds number and wind angle (ϕ) in relation to the length axis of the bluff body. Further more the model is capable of predicting an estimate for the structural damping needed for avoiding instability of the bluff body.

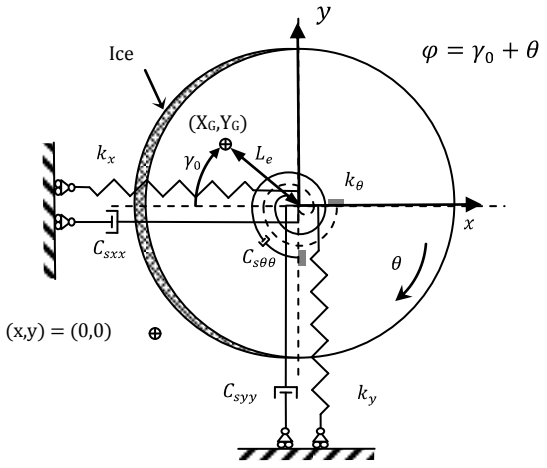

x	= displacement direction.
y	= displacement direction.
θ	= rotation direction.
γ_0	= angle offset for mass centre.
L_e	= mass centre offset.
k_x	= structural stiffness in x direction.
k_y	= structural stiffness in y direction.
k_θ	= structural damping in θ direction.
C_{sxx}	= structural damping in x direction.
C_{syy}	= structural damping in y direction.
$C_{s\theta\theta}$	= structural stiffness in θ direction.
(X_G,Y_G)	= mass centre.

Figure 1. Definition of system.

1 INTRODUCTION

The main purpose for models, which investigates aero-elastic behaviour, is to predict when aerodynamic instability occurs. During the last 80 years a number of models have been proposed and over the last couple of years aerodynamic damping, as a driving force for vibration, has received some renewed attention. Den Hartog proposed his stability criterion in 1932, Ref. [5], for a 1DOF system, which was defined for a bluff body with an aerodynamic lift coefficient formulated as a function of wind angle of attack in relation to the surface of the bluff body. Later, 1962, Davenport proposed an expression for the aerodynamic damping in the along wind and the transverse wind direction of a cylinder Ref. [3]. In 1981 Martin *et al.* proposed the instability criteria, which now is known under the name of "Drag instability" Ref. [7]. Up to that point all expressions for the aerodynamic damping were special cases, which should be applied individually. In 2006 a unified approach to damping and drag/lift instabilities was proposed by Macdonald and Larose Ref. [6] for a 1DOF system, which was later extended to a 2DOF system. This general quasi-steady 2DOF instability model is able to estimate the structural damping needed for avoiding instability of a bluff body moving in the XY-plane. The 2DOF model is capable of predicting the special cases, which earlier were applied individually, but lack the possibility of predicting inertial coupling for a bluff body with a mass centre offset from its rotational axis.

Through an ongoing research project on iced cables, which focuses on the different effects that ice accretions might have on the aerodynamic stability, it was found that torsion also played a vital role in the stability of a cable, Ref. [2], under certain conditions. This sparked the foundation for the idea to add the rotational dimension to the model developed by Macdonald and Larose in order to obtain a more comprehensive tool for analysing the stability of cables based on the quasi-static aerodynamic forces. In order to expand the model presented in Ref. [6] with an extra dimension it was necessary to find a quasi-static description of the rotational speed of the cable. Some research has been performed on torsional instability for models with different geometries and an approximation of the quasi-static rotational speed has been found for several geometries. A summary of this research can be found in Ref. [1] section 4.2.2. It is worth noticing that making a quasi-static description of the rotational speed seems to be difficult and according to the author's knowledge no unified expression, which clearly defines how to calculate the speed, has been devolved so far.

Using the research on an approximation to a quasi-static rotational speed, Ref. [1] section 4.2.2, it was possible to develop a new 3DOF quasi-steady model, which is proposed in this paper. This new 3DOF general quasi-static aerodynamic instability model incorporates the rotational movement of the cable and the coupling of all three degrees of freedom. In addition to prediction the instability of the cable in the XY-plane the new model is also capable of prediction instability due to the rotation of the cable and to predict instability due to a combination of movement in all the three degrees of freedom.

Furthermore, this new 3DOF general quasi-static aerodynamic instability model is also capable of estimating the damping need to suppress this instability. The model is able to predict the same levels of damping as the 2DOF model proposes by Macdonald et al. Additionally, it is capable of predicting the torsional damping needed to suppress instability and the combined damping need to suppress damping for an instability, which is a function of simultaneous motion in all three degrees of freedom.

2 THE MODEL

The bluff body model is based on a section model approach and developed for a cable with a thin ice accretion. The application of this model can be expanded to any geometry of a

prismatic bluff body subjected to aerodynamic instability. Figure 1, Figure 2 and Figure 3 shows the bluff body coordinate systems for load and structural respone, defined for a cable with a thin ice accretion.

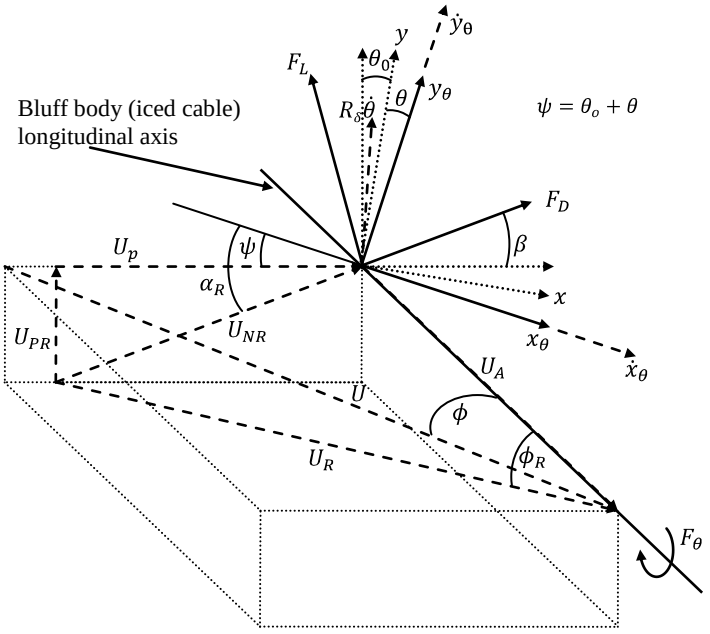

$x_\theta, \dot{x}_\theta$ = displacement, velocity.
$y_\theta, \dot{y}_\theta$ = displacement, velocity.
θ_0 = steady wind angle of attack
$\theta, \dot{\theta}$ = structural rotation, angular velocity.
α_R = wind angle of attack, cable surface.
β = angle of rotation, relative wind.
ϕ = wind angle of attack, cable length axis.
F_L = lift.
F_D = drag.
F_M = moment.
R_δ = Radial length for rotational speed.
δ = leading edge angle.
U = mean wind velocity.
U_R = relative wind velocity.
U_{PR} = projected relative vertical wind velocity.
U_p = projected relative horizontal wind velocity.
U_{NR} = normal projected relative wind velocity.
U_A = along axis wind velocity.

Figure 2. Schematic model of cable section with ice accretion.

The position of the ice accretion is described in the x-y coordinate system of the cross-sectional plane of the still body (Figure 3). If rotation is induced the angle θ describes the magnitude of rotation around the length axis of the bluff body.

Projected overall velocities

$$U_A = U\cos(\phi) \tag{1}$$

Relative velocities

$$\begin{aligned} U_P &= U\sin(\phi) - \dot{x}\cos(\psi) - \left(\dot{y}\sin(\psi) + R_\delta\dot{\theta}\sin(\delta)\right) \\ U_{PR} &= -\left(\dot{y}\cos(\psi) + R_\delta\dot{\theta}\cos(\delta)\right) + \dot{x}\sin(\psi) \\ U_{NR} &= \sqrt{(U_P^2 + U_{PR}^2)} \\ U_R &= \sqrt{(U_A^2 + U_{NR}^2)} \end{aligned} \tag{2}$$

Assumptions used in deriving the model:

- The model is based on a section model approach for a prismatic cable, which makes the assumption implying that the cable is straight and rigid at the midpoint of the cable.
- The ice shape is assumed to be prismatic.
- The structural damping is proportional to the velocity.
- The stiffness of the cable is constant.
- The overall wind speed, U, is constant.
- The rotational speed can be represented by motion of the leading edge point.
- Quasi-steady theory can be applied.

- Gravitational forces are not included.

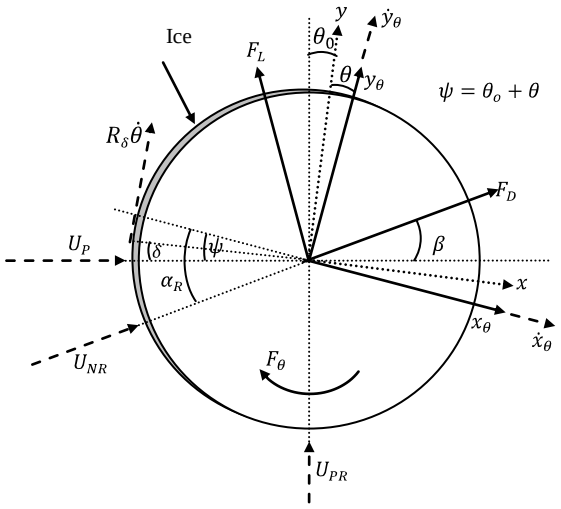

Figure 3. Analytical model of cable section with ice accretion.

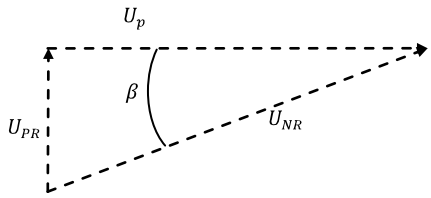

Figure 4. Definition of β.

Assumptions used in deriving the instability criterion:

- The cable is at rest at the initiation of the instability.
- Quasi-steady theory can be applied.

The instability criterion should only be used for a reduced velocity greater then $U/fD = 20$ due to the assumption of quasi-steady state and if the rotational degree of freedom is included then the criterion is limited to compact sections, see Ref. [1] section 4.2.2.

In the following the notation for time depended variables as $x(t), y(t)$ and $\theta(t)$ is written x, y and θ. Derivatives in respect to time are written as $(d/dt)x = \dot{x}$ and $(d^2/dt^2)x = \ddot{x}$

Both, the vertical and rotational motion of the cable section cause the angle of attack to vary over the section. For example, a positive rotational velocity induces a down draft forward of the centre of rotation and an updraft behind the centre of rotation and vice versa. The rotational velocity is approximated by the motion of a reference point defined in polar coordinates by the radial distance R_δ and angle δ as shown in Figure 3. As discussed in Ref. [1] section 4.2.2, the length R_δ is not directly related to characteristic points of the section geometry or of the flow field. It is rather a variable used to adjust the aerodynamic model output to the observed instabilities. For example for torsional instability of rectangles about the centroid R_δ has been approximated to half the distance between the centroid and the body's leading edge under the respective angle of attack. In the case discussed in this paper the length R_δ is chosen to be the length between the centre of rotation and to the leading edge of the model.

3 FORMULATION OF EQUATIONS

In deriving the equation of motion the energy approach has been applied using the Euler-Lagrange equation, see Eq. (3).

$$\begin{gathered}\frac{\partial}{\partial t}\left(\frac{\partial L}{\partial \dot{q}}\right)-\frac{\partial L}{\partial q}+DampForce=Force \\ L=T-V \qquad q=\{x,y,\theta\} \\ DampForce=\left\{C_{sxx}\dot{x},C_{syy}\dot{y},C_{s\theta\theta}\dot{\theta}\right\}\end{gathered} \tag{3}$$

where T is the kinetic energy of the system and V is the potential energy of the system.

3.1 Equations of motion

Figure 5 shows the coordinate system of the cable with ice accretion and illustrates the mass centre location of the model.

The dotted line shows the sign convention and the origin of the coordinate system $(0,0)$, which is the centre of the cable model shown in Figure 1. The point (x,y) is the displaced centre of the cable due to motion of the cable section in the *x*-*y*-plane. X_G and Y_G define the location of the mass centre of the cable section, where γ_0 and L_e are the polar coordinates of the mass centre in the *x*-*y*-plane and θ the additional angle due to rotation of the cable. The indices *Trans* and *Rot* refer to the movement of the mass centre due to translation and rotation respectively.

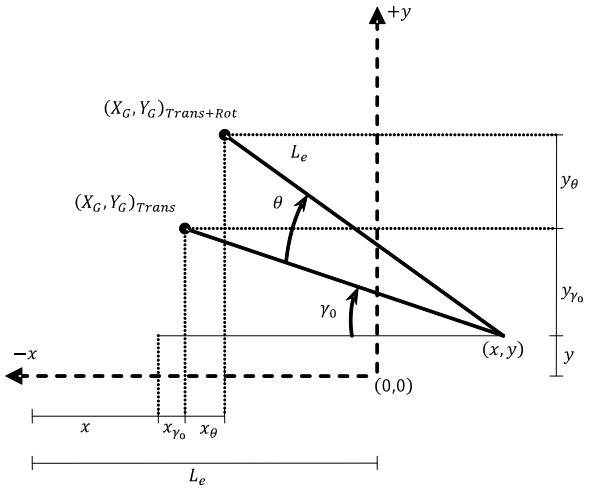

Figure 5. Definition of mass centre coordinates.

Eq. (4) and Eq. (5) gives the position for the mass centre of the cable.

$$X_G=x-L_e cos(\gamma_0+\theta) \tag{4}$$

$$Y_G=y+L_e sin(\gamma_0+\theta) \tag{5}$$

Using the Euler-Lagrange equation requires that one calculates the kinetic energy and potential energy according to the coordinate system shown in Figure 5. The obtained expressions for the energies are shown in Eq. (6) to Eq. (7).

$$T=\frac{1}{2}m_{tot}\left(\dot{X}_G^2+\dot{Y}_G^2\right)+\frac{1}{2}J\dot{\theta}^2 \tag{6}$$

$$V=\frac{1}{2}\left(k_x x^2+k_y y^2+k_\theta \theta^2\right) \tag{7}$$

where m_{tot} is the mass of the system and J is the rotational inertia about the mass centre.

Using the Euler-Lagrange approach results in obtaining the equation of motions (EOMs), which are given in Eq. (8) to Eq. (10).

$$m_{tot}\ddot{x} + C_{sxx}\dot{x} + k_x x + m_{tot}L_e\left(cos(\varphi)\,\dot{\theta}^2 + sin(\varphi)\,\ddot{\theta}\right) = F_x \tag{8}$$

$$m_{tot}\ddot{y} + C_{syy}\dot{y} + k_y y + m_{tot}L_e\left(-sin(\varphi)\,\dot{\theta}^2 + cos(\varphi)\,\ddot{\theta}\right) = F_y \tag{9}$$

$$(L_e^2 m_{tot} + J)\ddot{\theta} + C_{s\theta\theta}\dot{\theta} + k_\theta\theta + m_{tot}L_e(sin(\varphi)\,\ddot{x} + cos(\varphi)\,\ddot{y}) = F_\theta \tag{10}$$

F_x, F_y and F_θ are the external aerodynamic forces, which are presented in Eq. (11) to Eq. (13) for small initial displacements, where $\alpha_R = (\psi + \beta)$ and φ are given in Figure 3 and Figure 1, respectively.

The inertial coupling term for the x-direction, $\left(mL_e\cos(\varphi)\,\dot{\theta}^2 + mL_e\sin(\varphi)\,\ddot{\theta}\right)$, consists of two terms. The first coupling term is the centripetal force, $\left(mL_e\cos(\varphi)\,\dot{\theta}^2\right)$, and the second coupling term is the force originating from the angular acceleration, $\left(mL_e\sin(\varphi)\,\ddot{\theta}\right)$. Similar applies for the inertia coupling formulation in the y-direction. The inertial coupling in the θ-direction is based on tangential projections of the acceleration forces originating from the acceleration in the x- and y-direction.

$$F_x = \frac{1}{2}\rho U_R^2 D(C_D(\alpha_R, Re_R, \phi_R)\,cos(\alpha_R) + C_L(\alpha_R, Re_R, \phi_R)\,sin(\alpha_R)) \tag{11}$$

$$F_y = \frac{1}{2}\rho U_R^2 D(C_L(\alpha_R, Re_R, \phi_R)\,cos(\alpha_R) - C_D(\alpha_R, Re_R, \phi_R)\,sin(\alpha_R)) \tag{12}$$

$$F_\theta = \frac{1}{2}\rho U_R^2 D^2 C_M(\alpha_R, Re_R, \phi_R) \tag{13}$$

3.2 Aerodynamic damping

The instability criterion is based on a linearized version of the EOMs. This linearization is obtained by performing a Taylor expansion of the aerodynamic forces given in Eq. (11) to Eq. (13) to first order around the velocity of $\dot{x} = \dot{y} = \dot{\theta} = 0$.

$$\begin{aligned} F_Z(\dot{x},\dot{y},\dot{\theta})_{\dot{x}=\dot{y}=\dot{\theta}=0} &= F_Z + \frac{\partial F_Z}{\partial \dot{x}}\dot{x} + \frac{\partial F_Z}{\partial \dot{y}}\dot{y} + \frac{\partial F_Z}{\partial \dot{\theta}}\dot{\theta} + \frac{\partial F_Z}{\partial \dot{x}\partial \dot{y}}\dot{x}\dot{y} \\ &+ \dot{\theta}\left(\frac{\partial F_Z}{\partial \dot{x}\partial \dot{\theta}}\dot{x} + \frac{\partial F_Z}{\partial \dot{y}\partial \dot{\theta}}\dot{y} + \frac{\partial F_Z}{\partial \dot{x}\partial \dot{y}\partial \dot{\theta}}\dot{x}\dot{y}\right), where\ \left(F_Z = F_Z(0,0,0)\right) \end{aligned} \tag{14}$$

The Taylor expansion (Eq. (14)) of the aerodynamic forces results in a static wind force for all three directions and a dynamic force, which is equal to a Jacobian matrix (C_a) multiplied with the velocity in the three directions, $C_a\dot{Z}$ where $\dot{Z} = \left[\dot{x},\dot{y},\dot{\theta}\right]'$.

C_a is the aerodynamic damping matrix as given in eq. (15). The values of the aerodynamic damping matrix C_a are calculated for small initial displacements $(\cos(\theta) = 1,\ \sin(\theta) = 0)$ and found by applying an approach presented and discussed in Ref. [6].

$$C_a = -\begin{bmatrix} \frac{\partial F_x}{\partial \dot{x}} & \frac{\partial F_x}{\partial \dot{y}} & \frac{\partial F_x}{\partial \dot{\theta}} \\ \frac{\partial F_y}{\partial \dot{x}} & \frac{\partial F_y}{\partial \dot{y}} & \frac{\partial F_y}{\partial \dot{\theta}} \\ \frac{\partial F_\theta}{\partial \dot{x}} & \frac{\partial F_\theta}{\partial \dot{y}} & \frac{\partial F_\theta}{\partial \dot{\theta}} \end{bmatrix}_{\dot{x}=\dot{y}=\dot{\theta}=0} \tag{15}$$

Furthermore, it is assumed that all higher order terms in the EOMs are negligible. These assumptions derive from the instant where a vibration event is initiated on the body. Eq. (16) gives the total damping matrix containing both structural and aerodynamic damping.

$$C_D = C_s + C_a = \begin{bmatrix} C_{sxx} & 0 & 0 \\ 0 & C_{syy} & 0 \\ 0 & 0 & C_{s\theta\theta} \end{bmatrix} + \begin{bmatrix} C_{axx} & C_{axy} & C_{ax\theta} \\ C_{ayx} & C_{ayy} & C_{ay\theta} \\ C_{a\theta x} & C_{a\theta y} & C_{a\theta\theta} \end{bmatrix} = \begin{bmatrix} C_{xx} & C_{xy} & C_{x\theta} \\ C_{yx} & C_{yy} & C_{y\theta} \\ C_{\theta x} & C_{\theta y} & C_{\theta\theta} \end{bmatrix} \tag{16}$$

With these assumptions it is possible estimate the stability of the 3DOF system by rewriting the equations of motions (Eq. (8) to Eq. (10)) into state space and solving the eigenvalue problem which can be obtained here from.

Eq. (17) to Eq. (19) give the linearized version for the equations of motions Eq. (8) to Eq. (10), with the static aerodynamic force equal to zero, $\mathrm{F_Z} = 0$ where $\mathrm{Z} = [\mathrm{x}, \mathrm{y}, \theta]'$.

$$\ddot{x} = -\frac{1}{Jm_{tot}}\Big(J\big(m_{tot}\omega_x^2 x + C_{xx}\dot{x} + C_{xy}\dot{y} + C_{x\theta}\dot{\theta}\big) + sin(\varphi)L_e^2 m_{tot}\Big(-\frac{1}{L_e}\big(J\omega_\theta^2\theta + C_{\theta x}\dot{x} + C_{\theta y}\dot{y} + C_{\theta\theta}\dot{\theta}\big) + sin(\varphi)\big(\omega_x^2 m_{tot}x + C_{xx}\dot{x} + C_{xy}\dot{y} + C_{x\theta}\dot{\theta}\big) + cos(\varphi)\big(\omega_y^2 m_{tot}y + C_{yx}\dot{x} + C_{yy}\dot{y} + C_{y\theta}\dot{\theta}\big)\Big)\Big) \tag{17}$$

$$\ddot{y} = -\frac{1}{Jm_{tot}}\Big(J\big(m_{tot}\omega_y^2 y + C_{yx}\dot{x} + C_{yy}\dot{y} + C_{y\theta}\dot{\theta}\big) + cos(\varphi)L_e^2 m_{tot}\Big(-\frac{1}{L_e}\big(J\omega_\theta^2\theta + C_{\theta x}\dot{x} + C_{\theta y}\dot{y} + C_{\theta\theta}\dot{\theta}\big) + sin(\varphi)\big(\omega_x^2 m_{tot}x + C_{xx}\dot{x} + C_{xy}\dot{y} + C_{x\theta}\dot{\theta}\big) + cos(\varphi)\big(\omega_y^2 m_{tot}y + C_{yx}\dot{x} + C_{yy}\dot{y} + C_{y\theta}\dot{\theta}\big)\Big)\Big) \tag{18}$$

$$\ddot{\theta} = -\frac{1}{J}\Big(\big(J\omega_\theta^2\theta + C_{\theta x}\dot{x} + C_{\theta y}\dot{y} + C_{\theta\theta}\dot{\theta}\big) - L_e\big(sin(\varphi)\big(\omega_x^2 m_{tot}x + C_{xx}\dot{x} + C_{xy}\dot{y} + C_{x\theta}\dot{\theta}\big) + cos(\varphi)\big(\omega_y^2 m_{tot}y + C_{yx}\dot{x} + C_{yy}\dot{y} + C_{y\theta}\dot{\theta}\big)\big)\Big) \tag{19}$$

Below Eq. (20) shows the state-space matrix, which is obtained from Eq. (17) to Eq. (19)

$$\begin{bmatrix} 0 & 0 & 0 & 1 & 0 & 0 \\ 0 & 0 & 0 & 0 & 1 & 0 \\ 0 & 0 & 0 & 0 & 0 & 1 \\ & \vdots & & \vdots & \vdots & \vdots \\ \cdots & A & \cdots & B & C & D \\ & \vdots & & \vdots & \vdots & \vdots \end{bmatrix} \begin{bmatrix} x_1 \\ y_1 \\ \theta_1 \\ x_2 \\ y_2 \\ \theta_2 \end{bmatrix} = \begin{bmatrix} \dot{x}_1 \\ \dot{y}_1 \\ \dot{\theta}_1 \\ \dot{x}_2 \\ \dot{y}_2 \\ \dot{\theta}_2 \end{bmatrix} \tag{20}$$

Where A is a 3x3 sub-matrix, see Eq. (21), and B, C and D is a 3x1 sub-vector, see Eq. (22) to Eq. (24) and

(x_1, y_1, θ_1) represents the position of the cable section.
$(x_2, y_2, \theta_2) = (\dot{x}_1, \dot{y}_1, \dot{\theta}_1)$ represents velocity of the cable section.

$(\dot{x}_2, \dot{y}_2, \dot{\theta}_2) = (\ddot{x}_1, \ddot{y}_1, \ddot{\theta}_1)$ represents acceleration of the cable section.

$$A = \begin{bmatrix} -\frac{Jm_{tot}\omega_x^2 + sin(\varphi)^2 L_e^2 m_{tot}^2 \omega_x^2}{Jm_{tot}} & -\frac{cos(\varphi)sin(\varphi)L_e^2 m_{tot}\omega_y^2}{J} & sin(\varphi)L_e\omega_\theta^2 \\ -\frac{cos(\varphi)sin(\varphi)L_e^2 m_{tot}\omega_x^2}{J} & -\omega_y^2 - \frac{cos(\varphi)^2 L_e^2 m_{tot}\omega_y^2}{J} & cos(\varphi)L_e\omega_\theta^2 \\ \frac{sin(\varphi)L_e m_{tot}\omega_x^2}{J} & \frac{cos(\varphi)L_e m_{tot}\omega_y^2}{J} & -\omega_\theta^2 \end{bmatrix} \quad (21)$$

$$B = \begin{bmatrix} \frac{sin(\varphi)C_{\theta x}L_e}{J} - \frac{sin(\varphi)^2 C_{xx}L_e^2}{J} - \frac{cos(\varphi)sin(\varphi)C_{yx}L_e^2}{J} - \frac{C_{xx}}{m_{tot}} \\ \frac{cos(\varphi)C_{\theta x}L_e}{J} - \frac{cos(\varphi)sin(\varphi)C_{xx}L_e^2}{J} - \frac{cos(\varphi)^2 C_{yx}L_e^2}{J} - \frac{C_{yx}}{m_{tot}} \\ -\frac{C_{\theta x}}{J} + \frac{sin(\varphi)C_{xx}L_e}{J} + \frac{cos(\varphi)C_{yx}L_e}{J} \end{bmatrix} \quad (22)$$

$$C = \begin{bmatrix} \frac{sin(\varphi)C_{\theta y}L_e}{J} - \frac{sin(\varphi)^2 C_{xy}L_e^2}{J} - \frac{cos(\varphi)sin(\varphi)C_{yy}L_e^2}{J} - \frac{C_{xy}}{m_{tot}} \\ \frac{cos(\varphi)C_{\theta y}L_e}{J} - \frac{cos(\varphi)sin(\varphi)C_{xy}L_e^2}{J} - \frac{cos(\varphi)^2 C_{yy}L_e^2}{J} - \frac{C_{yy}}{m_{tot}} \\ -\frac{C_{\theta y}}{J} + \frac{sin(\varphi)C_{xy}L_e}{J} + \frac{cos(\varphi)C_{yy}L_e}{J} \end{bmatrix} \quad (23)$$

$$D = \begin{bmatrix} \frac{sin(\varphi)C_{\theta\theta}L_e}{J} - \frac{sin(\varphi)^2 C_{x\theta}L_e^2}{J} - \frac{cos(\varphi)sin(\varphi)C_{y\theta}L_e^2}{J} - \frac{C_{x\theta}}{m_{tot}} \\ \frac{cos(\varphi)C_{\theta\theta}L_e}{J} - \frac{cos(\varphi)sin(\varphi)C_{x\theta}L_e^2}{J} - \frac{cos(\varphi)^2 C_{y\theta}L_e^2}{J} - \frac{C_{y\theta}}{m_{tot}} \\ -\frac{C_{\theta\theta}}{J} + \frac{sin(\varphi)C_{x\theta}L_e}{J} + \frac{cos(\varphi)C_{y\theta}L_e}{J} \end{bmatrix} \quad (24)$$

It is through solving the eigenvalue problem for this linearized system of equations that it is possible to estimate the aerodynamic stability of a bluff body subjected to aerodynamic forces. The system of equations is stable if all the roots of the eigenvalue problem are below zero. The eigenvalue problem for this system of equations results in a 6th order polynomial, which can be solved either by numerical means or analytically by applying the Routh-Hurwitz stability criterion to the 6th order polynomial. By using the Routh-Hurwitz stability criterion it is also possible to differentiate whether the instability is characterised as diverged or flutter, Ref. [8].

4 PREDICTION OF INSTABILITY

The following describes the results found by the new 3DOF model proposed in this paper. Due to the limited number of wind tunnel experiments providing input data for the new model, the presented analysis focuses only on aerodynamic phenomena for wind normal to the cable axis. Previously performed analysis of 2DOF response in the *x*-*y*-direction is reported by Gjelstrup *et al.* in Ref. [4]

4.1 Aerodynamic data

Figure 6 shows the aerodynamic input data, used by the new model, which are taken from wind tunnel test performed by Chabart *et al* in 1998, Ref. [2]. The aerodynamic data are used in calculating the instability ranges, which are shown in Figure 8.

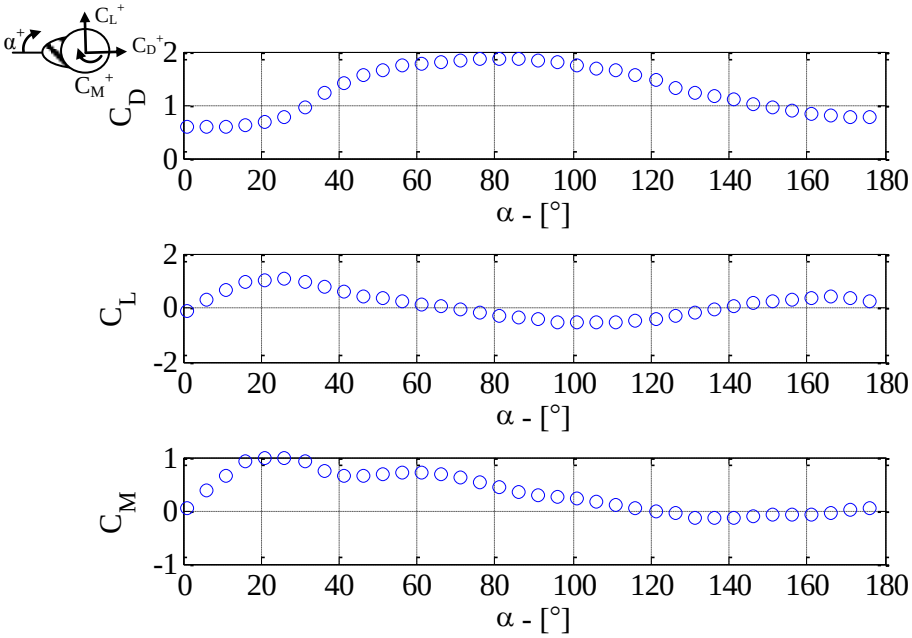

Figure 6. Aerodynamic coefficients taken from Ref. [2] and transformed into the model's coordinate system.

4.2 Calculated instability

Figure 7 shows a cross sectional view of the iced cable model from which the aerodynamic data were obtained. R_δ is the calculated individually for each angle of attack on the non-displaced body and used for the prediction of the instability range of the iced cable model.

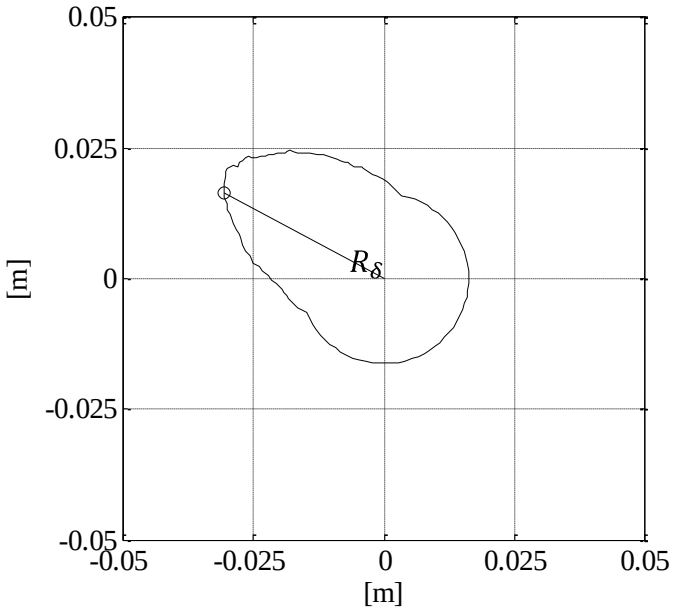

Figure 7. Iced cable with radial distance R_δ to the leading edge.

Figure 8a shows the calculated instability range found by using the aerodynamic data shown in Figure 6. Values less than zero indicate the ranges of instability predicted by the model. The unstable ranges are ~25° - ~45°, ~70° - ~135° and ~170° - 180°. Figure 8a also shows the Den Hartog criterion for instability, which states that galloping occurs, if $C_D + \partial C_L/\partial\alpha < 0$, where C_D and C_L are aerodynamic drag and lift coefficients and α is the wind angle of attack. The value of $C_D + \partial C_L/\partial\alpha$ is marked with a white line dotted with circles and the zero level for the Den Hartog criteria is marked with a straight white line, see Figure 8a. The Den Hartog criterion predicts instability in two ranges, 30° - 45° and 170° - 180°.

Comparing the results from these three approaches in Figure 8b it is demonstrated that the new model is capable of predicting instability over a wide range of wind angles of attack acting in a combined effect of drag lift and moment, which is not considered by previous models.

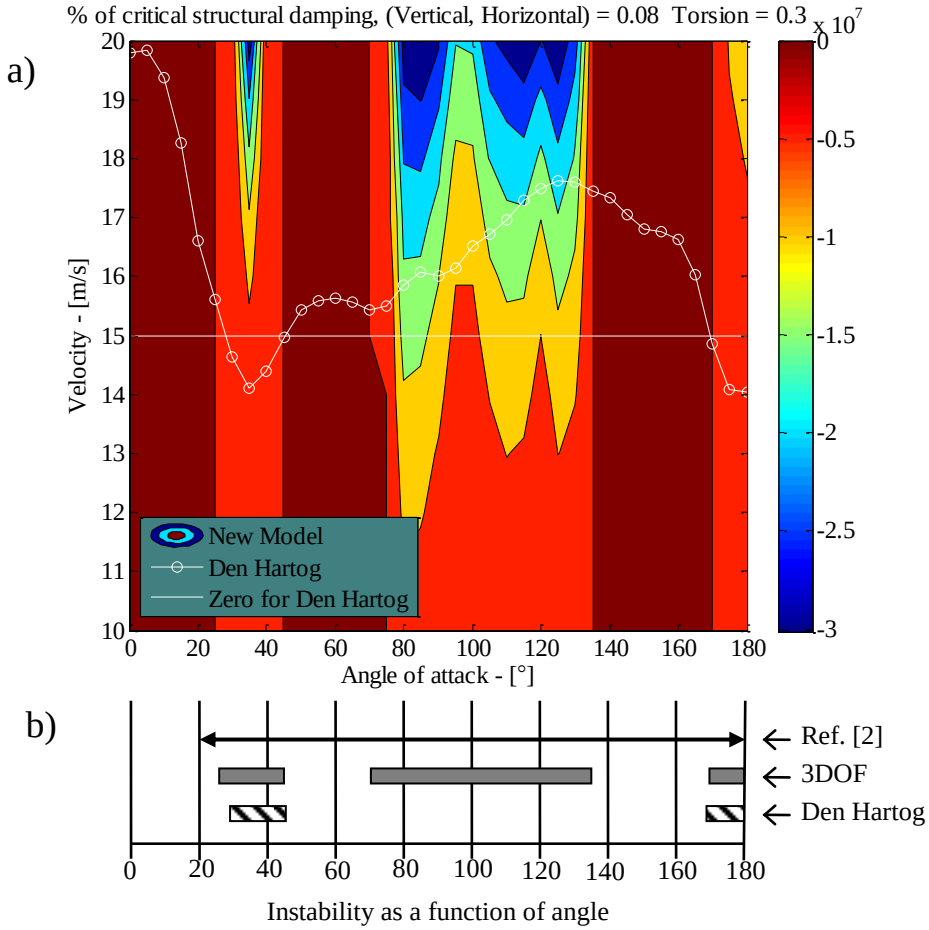

Figure 8. a) Range of predicted instability for the combined Drag, Lift and moment and $\gamma_0 = 0°$. b) Comparison of experimental found instability with Den Hartog and the 3DOF model

4.3 Discussion of results

Comparing the numerical found instability with results from previously made wind tunnel test, Ref. [2], good agreement between the experimental observed instability and the range predicted from the here presented model could be demonstrated. However the ranges from ~45° - ~70° and ~135° - ~170° are considered as stable in the numerical model, whereas the wind tunnel test, performed by Chabart *et al.* Ref. [2], shows that the model tested for different wind speeds and angles of attack was unstable in the entire range between 20° to 180°.

In comparison to older models designed with the aim to predict aerodynamic instability based on aerodynamic forces, this new model is able to predict instability over a wider range of wind angles.

REFERENCES

[1] R. D. Blevins. *Flow-Induced Vibration*, 2. Ed., Krieger, 1994.

[2] O. Chabart, and J. L. Lilien. "Galloping of electrical lines in wind tunnel facilities." *Journal of Wind Engineering and Industrial Aerodynamics*, 74-6, 967-976, 1998.

[3] A. G. Davenport. "Buffeting of suspension bridge by storm winds." *American Society of Civil Engineers -- Proceedings*, 88, 233-268, 1962.

[4] H. Gjelstrup, C. Georgakis, and A. Larsen. "A Preliminary Investigation of the Hanger Vibrations on the Great Belt East Bridge." Seventh International Symposium on Cable Dynamics, Vienna (Austria), 2007

[5] J. P. D. Hartog. "Transmission-Line Vibration Due to Sleet." *Institute of Electrical Engineers*, 51, 1074-1086, 1932.

[6] J. H. G. Macdonald, and G. L. Larose. "A unified approach to aerodynamic damping and drag/lift instabilities, and its application to dry inclined cable galloping." *Journal of Fluids and Structures*, 22,(2), 229-252, 2006.

[7] W. W. Martin, I. G. Currie, and E. Naudascher. "Streamwise oscillations of cylinders." *Journal of the Engineering Mechanics Division-Asce*, 107,(3), 589-607, 1981.

[8] J. J. Thomsen. *Vibrations and Stability*, Second Edition Ed., Springer, 2003.